UC Davis

UC Davis Previously Published Works

Title

Phase response properties of half-center oscillators

Permalink

https://escholarship.org/uc/item/9cb006k5

Journal

Journal of Computational Neuroscience, 35(1)

ISSN

0929-5313

Authors

Zhang, Calvin

Lewis, Timothy J

Publication Date

2013-08-01

DOI

10.1007/s10827-013-0440-1

Peer reviewed

eScholarship.org Powered by the California Digital Library
University of California

J Comput Neurosci (2013) 35:55–74
DOI 10.1007/s10827-013-0440-1

Phase response properties of half-center oscillators

Calvin Zhang · Timothy J. Lewis

Received: 17 June 2012 / Revised: 18 December 2012 / Accepted: 14 January 2013 / Published online: 28 February 2013
© Springer Science+Business Media New York 2013

Abstract We examine the phase response properties of half-center oscillators (HCOs) that are modeled by a pair of Morris-Lecar-type neurons connected by strong fast inhibitory synapses. We find that the two basic mechanisms for half-center oscillations, "release" and "escape", give rise to strikingly different phase response curves (PRCs). Release-type HCOs are most sensitive to perturbations delivered to cells at times when they are about to transition from the active to the suppressed state, and PRCs are dominated by a large negative peak (phase delays) at corresponding phases. On the other hand, escape-type HCOs are most sensitive to perturbations delivered to cells at times when they are about to transition from the suppressed to the active state, and PRCs are dominated by a large positive peak (phase advances) at corresponding phases. By analyzing the phase space structure of Morris-Lecar-type HCO models with fast synaptic dynamics, we identify the dynamical mechanisms underlying the shapes of the PRCs. To demonstrate the significance of the different shapes of the PRCs for the release-type and escape-type HCOs, we link the shapes of the PRCs to the different frequency modulation properties of release-type and escape-type HCOs, and we show that the different shapes of the PRCs for the release-type and escape-type HCOs can lead to fundamentally different phase-locking dynamics.

Keywords Central pattern generators (CPGs) · Half-center oscillators (HCOs) · Phase response curves (PRCs) · Phase plane analysis · Release and escape mechanisms

Action Editor: Frances K. Skinner

Electronic supplementary material The online version of this article (doi:10.1007/s10827-013-0440-1) contains supplementary material, which is available to authorized users.

C. Zhang · T. J. Lewis (✉)
Department of Mathematics, University of California, Davis, Davis, CA 95616, USA
e-mail: tjlewis@ucdavis.edu

C. Zhang
e-mail: jwzh@ucdavis.edu

1 Introduction

Central pattern generators (CPGs) are specialized neuronal circuits in the central nervous system that produce rhythmic activity in the absence of afferent feedback or rhythmic input (Hooper 2001; Marder and Calabrese 1996). Almost all rhythmic movements of animals (e.g., walking, swimming, breathing, chewing, etc.) are programmed at least in part by CPGs. While maintaining rhythmic activity, CPGs must be able to adjust their activity and respond appropriately (e.g., shift their phase or regulate their frequency) to input from higher centers and sensory feedback. Furthermore, behaviors such as locomotion are controlled by a network of interconnected CPG modules that interact to produce the limb or segmented-body movements necessary for effective locomotion, and therefore CPG modules must adjust their phases in response to input from other modules in order to produce the properly coordinated activity (Mulloney and Smarandache-Wellmann 2012; Cohen et al. 1992; Stein 2007). Thus, a comprehensive understanding of CPG activity must include an understanding of how they respond to input (Skinner et al. 1994; Nadim et al. 2011).

A useful way to characterize how oscillators respond to input is through their phase response curves (PRCs) (Schultheiss et al. 2012). PRCs measure the phase shift of an oscillator in response to a brief perturbation as a function of the timing of the input. PRCs in conjunction with coupled oscillators theory have been widely used in neuroscience to understand how changes in a neuron's intrinsic properties affect its frequency (Schwemmer and Lewis 2011; Ly and Ermentrout 2011), how neuronal oscillators phase-lock to external input (Brumberg and Gutkin 2007; Gouwens et al. 2010), and how networks of neurons synchronize (e.g., Ermentrout 1984; Hansel 1995; Mancilla 2007). In almost all cases, the oscillatory units have been taken to be the individual neurons. Despite the fact that oscillations in neural systems often arise from network interactions, there have been very few theoretical studies on the phase response properties of network-based oscillators (see however Ko and Ermentrout 2009; Schlichter 2011; Varkonyi et al. 2008; Jones et al. 2003). Furthermore, while coupled oscillator theory has been used extensively to study phase-locking in networks of CPGs, almost all of these studies have used a highly idealized model for the coupling (interaction) function (i.e., the phase model) (Cohen et al. 1992; Kopell and Ermentrout 1988; Williams et al. 1990; Skinner et al. 1994) rather than PRCs from biophysically-based models. It remains unclear how the intrinsic properties of cells and the synaptic coupling combine to produce the phase response properties of network-based oscillators and CPGs in particular.

In this article, we begin to explore the response properties of CPGs by examining the phase response characteristics of an idealized half-center oscillator (HCO) model. HCOs consist of two neurons (or neuronal populations) connected by reciprocal inhibition (Brown 1914; Mulloney and Smarandache 2010). This half-center organization is integral to many CPG circuits (e.g., Calabrese 1995; Satterlie 1985; Mulloney and Hall 2007; Smith et al. 2007). The reciprocal inhibition and some form of slow adaptation leads to antiphase oscillations in which the units alternate between an active state and a suppressed (inhibited) state. Two basic mechanisms for generating half-center oscillations have been described (Wang and Rinzel 1992; Skinner et al. 1994): "release" in which the oscillations are primarily controlled by the active cell releasing the suppressed cell from inhibition, and "escape" in which the oscillations are primarily controlled by the suppressed cell escaping from inhibition. We find that the release and escape mechanisms for Morris-Lecar-type HCO models give rise to strikingly different PRCs. We use geometric analysis of the phase portrait structure to explain how release and escape dynamics shape the PRCs, and we then give examples of how the shapes of the PRCs can lead to fundamentally different responses to external input.

2 Methods

2.1 Description of half-center oscillator model

The model half-center oscillator (HCO) used in this study consists of two neurons that are strongly coupled by fast reciprocal inhibitory synapses. Specifically, we use the HCO model described by Skinner et al. (1994). The dynamics of each neuron are described by standard current balance equations based on the Morris-Lecar model (Morris and Lecar 1981). For the phase portrait arguments and the numerical simulations presented in the main text, the cells are taken to be *non-oscillatory* when isolated. The ionic currents in the model cells include a rapidly activating inward current (the "calcium" current), an outward current with relatively slow activation kinetics (the "potassium" current) and a voltage-independent leakage current. The strong inhibitory synapses are modeled as "fast threshold modulation" synapses (Somers and Kopell 1993). Note that the model does not include ionic currents that underlie fast spikes. Therefore, the voltage of the model during the active state can be interpreted as the actual membrane potential of a non-spiking cell, or it can be interpreted as the voltage "envelope" during a burst of action potentials in a spiking neuron.

The model equations are

$$C\frac{dV_i}{dt} = I - g_{\mathrm{Ca}} m_\infty(V_i)\big(V_i - E_{\mathrm{Ca}}\big) - g_{\mathrm{K}} n_i\big(V_i - E_{\mathrm{K}}\big) - g_L\big(V_i - E_L\big) - I_{\mathrm{syn},j\to i} + I_{\mathrm{ext},i}(t), \tag{1}$$

$$\frac{dn_i}{dt} = \frac{\epsilon_n}{\tau_n(V_i)}\big(n_\infty(V_i) - n_i\big), \tag{2}$$

where V_i is the membrane potential for cell i, and n_i is the gating variable for the potassium current in cell i ($i, j = 1, 2; i \neq j$). C is the membrane capacitance; g_{Ca}, g_{K} and g_{L} are the maximal conductances, and E_{Ca}, E_{K} and E_{L} are the reversal potentials for the calcium, potassium and leakage currents, respectively. I is a bias current (which could be absorbed into E_{L}), and $I_{\mathrm{ext},i}$ is an external current injected into cell i. The functions $m_\infty(V)$ and $n_\infty(V)$ describe the voltage-dependent steady state activation curves for the calcium and potassium conductances

$$m_\infty(V) = \frac{1}{2}\Big[1 + \tanh\Big(\frac{V - V_a}{V_b}\Big)\Big], \tag{3}$$

$$n_\infty(V) = \frac{1}{2}\Big[1 + \tanh\Big(\frac{V - V_c}{V_d}\Big)\Big], \tag{4}$$

and $\frac{\tau_n(V)}{\epsilon_n}$ is the time constant for potassium conductance activation in which

$$\tau_n(V_i) = \cosh^{-1}\Big(\frac{V - V_c}{2V_d}\Big). \tag{5}$$

The activation dynamics for the calcium conductance ($m_\infty(V)$) is taken to be an instantaneous function of the membrane potential. The level of activation of the potassium conductance (n) is modeled as a dynamic variable to capture its relatively slow response to changes in the membrane potential, which can be controlled by scaling the factor ϵ_n.

The fast synaptic current imposed by neuron j onto neuron i is

$$I_{\text{syn},\,j\to i} = g_{\text{syn}} s_\infty(V_j)\big(V_i - E_{\text{syn}}\big), \tag{6}$$

where g_{syn} and E_{syn} are the maximal conductance and the reversal potential for the synaptic currents, respectively. The synaptic conductances are assumed to have fast dynamics and are taken to be instantaneous functions of the membrane potential of the presynaptic neuron (V_{pre}). Specifically, the level of activation of the synapses is given by the monotonically increasing sigmoid function

$$s_\infty(V_{\text{pre}}) = \frac{1}{2}\Big[1 + \tanh\Big(\frac{V_{\text{pre}} - \eta_{\text{syn}}}{k_{\text{syn}}}\Big)\Big], \tag{7}$$

where η_{syn} is the membrane potential at which the synaptic conductance is half-maximal, and k_{syn} determines the steepness of the synaptic activation curve $s_\infty(V_{\text{pre}})$. The synaptic activation curve is assumed to be steep, i.e., k_{syn} is small. Therefore, we interpret η_{syn} as the "synaptic threshold".

All simulations of the Morris-Lecar-based HCO model were performed using the same parameter values as Skinner et al. (1994) except for ϵ_n and k_{syn}. (We relax their assumptions that the parameters ϵ_n and k_{syn} are extremely small). Unless otherwise stated, $C = 1\ \mu\text{F/cm}^2$, $g_{\text{Ca}} = 0.015$ mS/cm^2, $E_{\text{Ca}} = 100$ mV, $g_{\text{K}} = 0.020$ mS/cm^2, $E_{\text{K}} = -80$ mV, $g_{\text{L}} = 0.005$ mS/cm^2, $E_{\text{L}} = -50$ mV, $g_{\text{syn}} = 0.010$ mS/cm^2, $E_{\text{syn}} = -80$ mV, $V_a = 0$ mV, $V_b = 15$ mV, $V_c = 0$ mV, $V_d = 15$ mV, $\epsilon_n = 0.0005$, $k_{\text{syn}} = 2$ mV, and η_{syn} is defined in each example. $I_{\text{ext},i}(t) = 0$ ($i = 1, 2$) except when studying the effects of small perturbations or periodic inputs to the HCO model. The bias current $I = 0.8\ \mu\text{A/cm}^2$, except when it is varied to show how it affects the phase response properties of the HCO (see Section 3.3).

The generality of our analysis suggests that our basic results carry over to all Morris-Lecar-type HCO models with fast synapses (i.e., the family of models with similar phase space structure to the Morris-Lecar-based HCO model described here) and do not depend on the specific combination of parameters used in our model or the specific choice of the Morris-Lecar-type models. We support this claim by presenting the PRCs and phase portraits for different cases in the appendices. Appendix A shows that the results for Morris-Lecar-based HCOs with intrinsically oscillatory dynamics are similar to those for Morris-Lecar-based HCOs with intrinsically non-oscillatory cells presented in the main text. Appendix B shows that similar results also hold for the Wang-Rinzel (HCO) model (Wang and Rinzel 1992).

2.2 Phase response curves

A phase response curve (PRC) quantifies the sensitivity of an oscillator at different phases in its cycle (Schwemmer and Lewis 2012). Specifically, the PRC of a neuronal oscillator measures its phase shift in response to a brief current pulse as a function of the phase at which the pulse is delivered. The convention adopted in this article is that a phase advance is indicated by a positive value on the PRC, whereas a phase delay is indicated by a negative value. If the current pulse amplitude is sufficiently small and its duration is sufficiently brief, then the phase shift will be proportional to the total charge injected during the pulse. In this case, when the phase shift is normalized by the total charge and membrane capacitance, one obtains the "infinitesimal PRC", which has units of time per unit membrane potential (msec/mV). In what follows, we use "PRC" to refer to the infinitesimal PRC, which we denote by $Z(\theta)$ where θ is the phase of the oscillator (in units of time), and T is the period of the oscillation.

In neuroscience applications, PRCs typically are determined for single oscillatory neurons, but they can also be used to characterize the response properties of neural systems in which oscillations arise from network properties. Note that despite the fact that a network-based oscillator contains more than one cell, the oscillator has a single phase, θ. However, perturbations can be delivered to each cell in the network, and hence there is a different PRC for each neuron. For our HCO model, which consists of two identical neurons oscillating in anti-phase, the PRCs for each neuron are identical except for a phase shift of a half-period ($0.5T$). We define the PRC for cell 1 to be $Z_1(\theta) = Z(\theta)$, and then the PRC for cell 2 is $Z_2(\theta) = Z(\theta + 0.5T)$.

PRCs for individual neurons and neuronal networks can be obtained directly by applying brief current pulses at many different times in the oscillator's cycle and measuring the subsequent change in timing of the next spike (e.g., Mancilla et al. 2007; Smarandache et al. 2009; Netoff et al. 2012). PRCs for mathematical models can also be computed by solving the adjoint equations for the full model equations linearized around the system's T-periodic limit cycle. The PRCs for the HCO model (Eqs. (1) and (2)) presented in this article are computed using this so-called adjoint method as described by Williams and Bowtell (1997). However, example PRCs were checked against PRCs that were obtained by using the direct method. See Appendix C for a comparison of infinitesimal PRC computed using the adjoint method and PRCs computed using the direct method.

2.3 Phase models

Besides characterizing the phase-dependent sensitivity of the HCO, the PRC can be used to examine the oscillator's phase-locking dynamics in response to periodic external input. Using the theory of weakly coupled oscillators (Kuramoto 1984; Malkin 1949; Ermentrout 1984), the dynamics of the HCO can be reduced to the consideration of a "phase model", in which the state of the oscillator is described entirely by its phase $\theta(t)$. The phase can be decomposed into two parts: $\theta(t) = \big(t + \phi(t)\big) \mod T$, where t describes the change in the phase of the oscillator in the absence of the external input, and the relative phase $\phi(t)$ quantifies the phase shift that results from the external input. If the effect of the T-periodic external input on the phase of the oscillator is relatively small compared to that of the intrinsic dynamics of the oscillator, then the change in $\phi(t)$ is very small (negligible) over a single period, i.e., $\phi(t)$ is approximately constant over a single period. However, these small changes in $\phi(t)$ can accumulate over many periods to produce significant phase shifts. This slow-time evolution of $\phi(t)$ for the HCO is captured by the phase equation

$$\frac{d\phi}{dt} = H_1(\phi) + H_2(\phi) \equiv H(\phi), \tag{8}$$

where

$$H_i(\phi) = \frac{1}{T}\int_0^T Z_i(s+\phi)\frac{I_{\text{ext},i}(s)}{C}ds.$$

The interaction function $H_i(\phi)$ quantifies the average rate of change of the relative phase of the HCO over a period T that results from the external input into cell i at any particular relative phase ($\phi \approx$ constant within a single period). The phase Eq. (8) is a first-order autonomous differential equation that can be easily analyzed. Specifically, the zeros of $H(\phi)$ correspond to the steady states of the phase model and therefore the phase-locked states of the oscillator subject to the external T-periodic input $I_{\text{ext},i}(t)$. These phase-locked states are stable if $\frac{dH(\phi)}{d\phi} < 0$. Note that the above mathematical framework can be extended to accommodate the case in which the external forcing is not strictly T-periodic and to study the phase-locking properties of coupled oscillator networks. Details of the theory of weakly coupled oscillators can be found in the recent review by Schwemmer and Lewis (2012).

3 Results

In this section, we first review the basic dynamics of half-center oscillations (Wang and Rinzel 1992; Skinner et al. 1994) and show that the phase response curves (PRCs) for the release-type and the escape-type half-center oscillators (HCOs) have strikingly different shapes. We then explain how the shapes of the PRCs arise from the basic dynamics of the HCO under the release and escape mechanisms. Finally, we provide examples that demonstrate how the shapes of the HCO's PRC can be used to understand the effect of external constant input on the HCO's frequency and how the HCO phase-locks to periodic input.

3.1 PRCs of HCOs under "release" and "escape" mechanisms have different shapes

3.1.1 The basic dynamics of HCOs

An HCO consists of two non-oscillatory cells that are coupled by mutual inhibition. The fast synaptic inhibition and the rapid calcium-current kinetics interact with the slow potassium-current kinetics to produce anti-phase oscillations in which the cells transition between an active state and a suppressed (inhibited) state. If the cells' transition between the active state and the suppressed state is triggered by changes in the active cell, the underlying mechanism is called "release". If the transition is triggered by changes in the suppressed cell, it is called "escape". In this subsection, we briefly describe the dynamics for these two types of HCO mechanisms. For simplicity, we present idealized cases in which the cells in the HCO are assumed to undergo relaxation-oscillator-like dynamics (i.e., relatively small ϵ_n) and the synapses connecting the cells are assumed to have a sharp threshold for the activation (i.e., small k_{syn}) (Skinner et al. 1994). However, we show that the basic behavior and main conclusions in the article carry over to less restrictive cases.

Release Mechanism Figure 1a plots the membrane potentials V_i and the gating variables for the outward K^+ current n_i as functions of phase for cell 1 and cell 2 during steady half-center oscillations under the release mechanism. Points A, B, C, D and A', B', C', D' indicate landmark points in the half-center oscillations for cell 1 and cell 2, respectively. At phase $\theta = 0$, cell 1 has just made a transition from the suppressed state to the active state. Its membrane potential V_1 is at a maximal value (point A) that is above the synaptic threshold η_{syn}, and therefore cell 1 is inhibiting cell 2. Cell 2 has just been driven from the active state to the suppressed state by the inhibition from cell 1, and V_2 is at a minimal membrane potential (point C'), which is well below η_{syn}. As the cycle progresses, the outward K^+ current slowly activates in cell 1 (i.e., n_1 slowly increases in an exponential fashion), leading to a slow exponential decrease in V_1 (A $\rightarrow$ B). On the other hand, the outward K^+ current in cell 2 slowly deactivates (i.e., n_2 slowly decreases in an

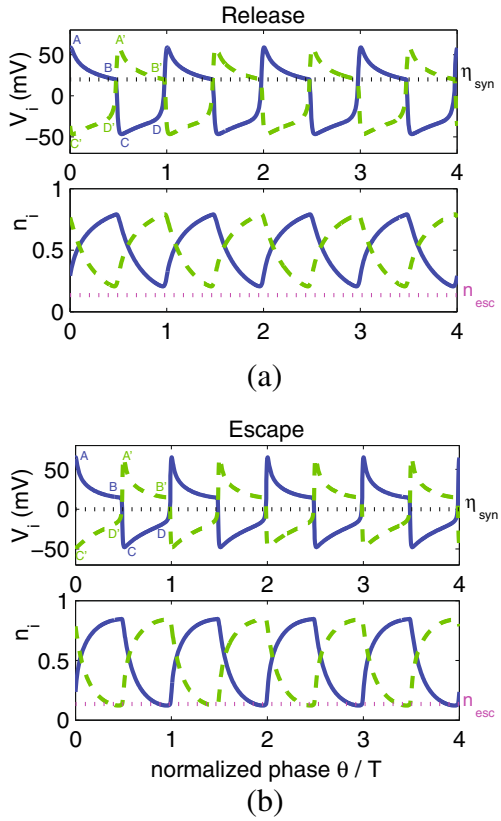

Fig. 1 Dynamics of HCOs. **a** A release-type HCO ($\eta_{\text{syn}} = 20$ mV). **b** An escape-type HCO ($\eta_{\text{syn}} = 0$ mV). In both (**a**) and (**b**), the top figures show the membrane potential V_i of cell 1 (*solid curve*) and cell 2 (*dashed curve*) as functions of the phase (normalized by the period T), where the horizontal dotted line is the "synaptic threshold" η_{syn}, and the bottom figures show the gating variable n_i of cell 1 (*solid curve*) and cell 2 (*dashed curve*) as functions of the phase, where the horizontal dotted line indicates the "escape threshold" n_{esc}. Markers A, B, C and D indicate landmark points in the half-center oscillations of cell 1, whereas A', B', C', D' indicate the corresponding points for cell 2. These markers are referenced throughout the main text

exponential fashion), leading to a slow exponential depolarization of cell 2 (C' → D'). If the active cell 1 were isolated, it would asymptotically approach a depolarized steady state at $V_1 = 13$ mV, $n_1 = 0.85$. However, as V_1 decreases toward this steady state, it crosses η_{syn} immediately before phase $\theta = 0.5T$ (point B), which turns off the inhibitory synapse from cell 1 to cell 2. Upon its release from inhibition, cell 2's membrane potential V_2 rapidly depolarizes and rises above η_{syn} (D' → A'). Cell 1 is now inhibited, and V_1 rapidly hyperpolarizes (B → C). Thus, at $\theta = 0.5T$, cell 1 and cell 2 have switched states after half of the period; cell 2 is now in the active state with V_2 at a maximal value (point A') and cell 1 is now in the suppressed state with V_1 at a minimal value (point C). The second half of the cycle (θ from $0.5T$ to T) is identical with the two cells' roles switched.

Escape Mechanism Figure 1b shows the dynamics of the HCO under the escape mechanism. At phase $\theta = 0$, cell 1 is at its maximal membrane potential (point A) and is inhibiting cell 2, which is at its minimal membrane potential (point C'). As described for the release-type HCO, as the cycle progresses (θ from 0 to $0.5T$), cell 1 slowly exponentially repolarizes (A → B), while cell 2 slowly exponentially depolarizes (C' → D'). If cell 1 remains uninhibited, it would asymptotically approach a depolarized steady state at $V_1 = 13$ mV, $n_1 = 0.85$. However, in the escape-type HCO, soon before phase $\theta = 0.5T$, the gating variable n_2 for the outward K^+ current in cell 2 decreases to a critical value $n_{\text{esc}} = 0.13$ below which the fast inward current is greater than the outward current. This leads to the rapid depolarization of cell 2 (D' → A'), while it is still inhibited by cell 1. We refer to the critical value n_{esc} as the "escape threshold". Upon its escape from inhibition, cell 2's membrane potential V_2 rises above the synaptic η_{syn}, which turns on the synaptic inhibition from cell 2 to cell 1. The inhibition from cell 2 causes cell 1 to rapidly hyperpolarize (B → C), and V_1 falls below η_{syn}, turning off the synaptic input from cell 1 to cell 2. Cell 2 finally reaches the maximal membrane potential (point A'). Thus, at phase $\theta = 0.5T$, cell 1 and cell 2 have switched states. The second half of the cycle (θ from $0.5T$ to T) is identical to the first half of the cycle but the roles of the two cells are switched.

Note that, for the release-type HCO (Fig. 1a), the gating variable for the slow outward K^+ current n_i never falls below the escape threshold n_{esc}. The cells' transition between the active and suppressed states does not rely on the intrinsic dynamics of the suppressed cell. Instead, the timing of the transition is controlled by the membrane potential of the active cell falling below the synaptic threshold η_{syn} and releasing the suppressed cell from inhibition. On the other hand, for the escape-type HCO (Fig. 1b), dynamics of the active cell and the exact value of η_{syn} does not play a role in initiating the transition of the cells between the active and suppressed states. The timing of the transition is controlled by the intrinsic properties of the suppressed cell. Specifically, as the gating variable of the suppressed cell drops below n_{esc}, the fast inward current overcomes the slow outward current, leading to a rapid depolarization of the suppressed cell and its escape from inhibition. For more general and detailed descriptions of HCO dynamics and the release and escape mechanisms, see Wang and Rinzel (1992), Skinner et al. (1994) and Daun et al. (2009).

3.1.2 PRCs of HCOs

Figures 2a and b show the PRCs and the corresponding membrane potentials of HCOs under the release and the escape mechanisms, respectively. Recall that because the

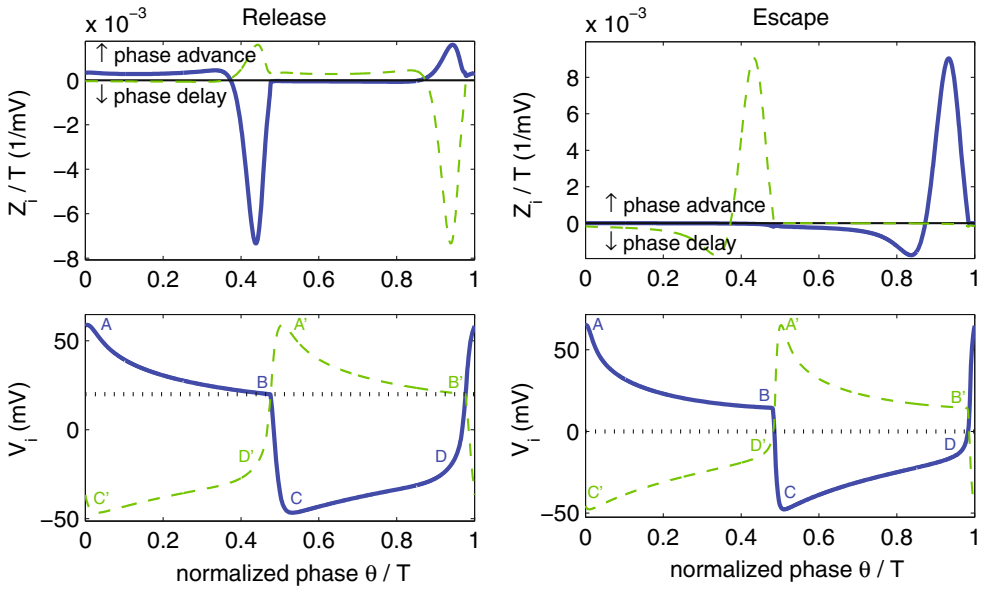

Fig. 2 PRCs for release-type and escape-type HCOs have strikingly different shapes. **a** The PRC of a release-type HCO ($\eta_{\text{syn}} = 20$ mV).**b** The PRC of an escape-type HCO ($\eta_{\text{syn}} = 0$ mV). In both (**a**) and (**b**), the top figure shows the PRCs of cell 1 (*solid curve*) and cell 2 (*dashed curve*), and the bottom figures shows the corresponding membrane potential of cell 1 (*solid curve*) and cell 2 (*dashed curve*) as functions of the phase. The horizontal dotted line in the bottom figures indicates the synaptic threshold η_{syn}. At phases when $Z_i > 0$, the HCO will advance its phase in response to small brief positive current pulses delivered to cell i; whereas when $Z_i < 0$, the HCO will delay its phase in response to these stimuli. The PRC of a release-type HCO is dominated by a large negative peak late in the first half of the cycle, whereas the PRC of an escape-type HCO is dominated by a large positive peak late in the second half of the cycle. Markers A, B, C, D for cell 1 and A', B', C', D' are used to indicate landmark points as in Fig. 1

two cells in the HCO are in anti-phase, the PRC obtained when cell 1 is perturbed ($Z_1(\theta) = Z(\theta)$) and the PRC obtained when cell 2 is perturbed ($Z_2(\theta) = Z(\theta + 0.5T)$) are identical except for a half-period phase shift. Therefore, we will describe only the PRC for cell 1, and refer to it as "the PRC of the HCO".

The PRCs for the two half-center oscillation mechanisms have strikingly different shapes. Most notably, the PRC for the release mechanism is dominated by a large negative peak late in the first half of the period, whereas the PRC for the escape mechanism is dominated by a large positive peak late in the second half of the period. This implies that a brief positive applied current pulse delivered to cell 1 (i.e., a ΔV perturbation to V_1) late in the first half of the period will significantly delay the phase of a release-type HCO, but it will do little to an escape-type HCO. On the other hand, the same ΔV perturbation delivered late in the second half of the period will significantly advance the phase of an escape-type HCO, but it will have a much smaller effect on a release-type HCO. Note that, despite their very different PRCs, HCOs under the release and escape mechanisms can have very similar membrane potential traces (see the bottom figures in Fig. 2a, b or Fig. 1). This suggests that it is difficult to predict an HCO's phase response properties simply by examining the membrane potential, and it is difficult to assess whether the release or escape mechanism underlies the half-center oscillations by examining the membrane potential alone (i.e., without knowing the synaptic threshold and the escape threshold), but the oscillation mechanism is clear from the shape of the PRC.

The basic shapes of PRCs for the release and escape mechanisms persist as ϵ_n and k_{syn} vary. The left figure in Fig. 3 shows the PRCs of escape-type HCOs with several values of ϵ_n and fixed $k_{\text{syn}} = 2.0$. The dominant positive peak late in the second half of the period is preserved, and in fact, it becomes taller and broader as ϵ_n increases (i.e., as the dynamics of the system become less relaxation-oscillator-like). Note also that the shape of the PRC for the escape-type HCO is insensitive to changes in k_{syn} (not shown), because the escape-type half-center oscillations are largely controlled by the intrinsic properties of the suppressed cell rather than the synaptic activation threshold (see Section 3.1; Wang and Rinzel 1992; Skinner et al. 1994). The middle figure in Fig. 3 shows the PRCs of release-type HCOs with several values of k_{syn} and a fixed $\epsilon_n = 0.0005$. The dominant negative peak late in the first half of the period, which is characteristic of the PRCs for the release mechanism, is preserved. The right figure in Fig. 3 shows

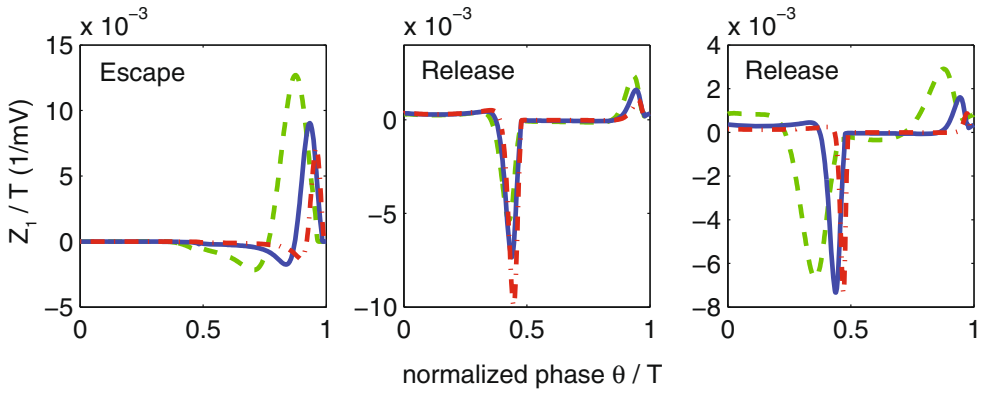

Fig. 3 PRCs of HCOs with different values of ϵ_n and k_{syn}. Left figure: $\eta_{\text{syn}} = 0$ mV (*all PRCs*), $k_{\text{syn}} = 2.0$ (*all PRCs*); $\epsilon_n = 0.0020$ (*dashed curve*), $\epsilon_n = 0.0005$ (*solid curve*), $\epsilon_n = 0.0002$ (*dash-dotted curve*). *Middle figure*: $\eta_{\text{syn}} = 20$ mV (*all PRCs*), $\epsilon_n = 0.0005$ (all PRCs); $k_{\text{syn}} = 4$ (*dashed curve*), $k_{\text{syn}} = 2$ (*solid curve*), $k_{\text{syn}} = 1$ (*dash-dotted curve*). *Right figure*: $\eta_{\text{syn}} = 20$ mV (*for all PRCs*); $\epsilon_n = 0.0020$ and $k_{\text{syn}} = 4$ (*dashed curve*), $\epsilon_n = 0.0005$ and $k_{\text{syn}} = 2$ (*solid curve*), $\epsilon_n = 0.0002$ and $k_{\text{syn}} = 1$ (*dash-dotted curve*). The left figure is based on the escape-type HCO, whereas the two figures on the right are based on the release-type HCO. The solid curve in the left figure is the same PRC shown in Fig. 2b. The solid curves in the two figures on the right are the same PRC shown in Fig. 2a

the PRCs of release-type HCOs when ϵ_n and k_{syn} are varied simultaneously. Once again, the basic shape of the PRC is preserved, but larger values of both parameters combine to make the negative peak broader. Furthermore, the small "escape-like" positive peak in the second half of the period increases in size.

Note that the PRCs presented above are infinitesimal PRCs. With stronger perturbations, the shape of the PRC may depend on the magnitude and the sign (excitatory or inhibitory) of the perturbation. In Appendix C, we compare the infinitesimal PRCs for the Morris-Lecar-based HCOs with the PRCs directly computed by injecting finite strength delta function perturbations into one of the cells. We find that the shape of the infinitesimal PRC is very close to the shapes of PRCs computed using delta-function perturbations with at least up to 5 mV stimulus strength.

Furthermore, in Appendix A and B, we show that the PRCs for the Wang-Rinzel (HCO) model and Morris-Lecar-based HCOs with intrinsically oscillatory cells have the same basic shapes as those described in this section.

3.2 Mechanisms by which release and escape dynamics shape the HCO's PRC

In this subsection, we identify the general dynamical properties of Morris-Lecar-type HCO models that give rise to the shapes of the HCOs' PRCs. Specifically, we describe how perturbations to cell 1's membrane potential ΔV at different phases θ lead to the changes in the time Δt for the perturbed cell to reach the critical threshold in the half-center oscillations (i.e., the synaptic threshold η_{syn} for release-type HCOs or the escape threshold n_{esc} for escape-type HCOs) and ultimately how these changes in timing result in the asymptotic phase shift $\Delta\theta$ of the HCO. Note that the changes in timing Δt as a function of the phase θ that the perturbation is delivered (normalized by the total charge of the perturbation over the membrane and the intrinsic period of the HCO) is the "first order PRC" (Netoff et al. 2012).

Our explanations use the idealizations of relaxation-oscillator-like dynamics for the individual neurons (relatively small ϵ_n) and a sharp synaptic threshold (small k_{syn}). Recall that: (1) The sharp threshold ensures that the active cell receives no inhibitory synaptic input, whereas the suppressed cell is subject to a maximal constant inhibitory synaptic conductance. (2) The relaxation-oscillator-like dynamics ensure that the transitions between the active and suppressed states are relatively rapid, so cells are almost always in one of these two states at all times. Note, however, the basic results hold when these restrictions are relaxed. Given the assumptions of small ϵ_n and k_{syn}, the only essential dynamical property that our explanation requires is the exponential deceleration of the cells' state as they progress through the active and suppressed states. This property is typical for Morris-Lecar-type systems with relaxation-oscillator-like dynamics (Rinzel and Ermentrout 1989).

To aid the explanation of how the dynamics of HCOs shape their phase response properties, we use the phase portraits of the half-center oscillations projected onto the (V, n) phase plane. Because the two cells in the HCO model are identical and firing in anti-phase, we can use the two-dimensional (V, n) phase plane to understand the dynamics of the 4-dimensional system (Skinner et al. 1994; Wang and Rinzel 1992; Daun et al. 2009). Figure 4 shows the (V, n) phase plane for (a) a release-type HCO and (b) an escape-type HCO. The n-nullcline ($n = n_\infty(V)$; dash-dotted curve) is monotonically increasing in V. Because of

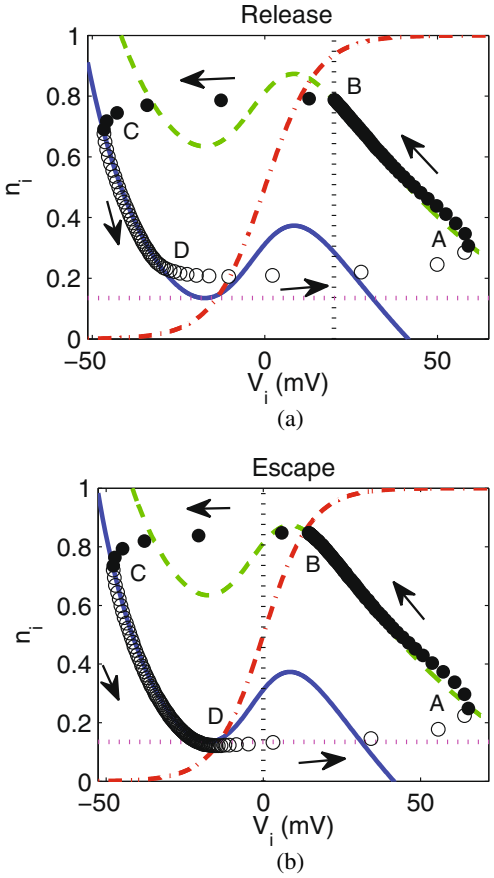

Fig. 4 HCO dynamics in the (V, n) phase plane. **a** A release-type HCO ($\eta_{\text{syn}} = 20$ mV). **b** An escape-type HCO ($\eta_{\text{syn}} = 0$ mV). Solid curve: the V-nullcline when a cell is fully inhibited. *Dashed curve*: the V-nullcline when a cell is fully uninhibited. dash-dotted curve: the n-nullcline, which is not dependent on the status of the presynaptic cell. Solid dots: cell 1's trajectory evenly spaced in time for the first half of the cycle. Open circles: cell 1's trajectory evenly spaced in time for the second half of the cycle. The vertical dotted line indicates the synaptic threshold η_{syn}. The horizontal dotted line indicates the escape threshold n_{esc} (the value of the gating variable n at the lower left knee of the fully inhibited V-nullcline). Markers A, B, C, D indicate the landmark points for cell 1, which correspond to A, B, C, D in Fig. 1 and Fig. 2

the sharp threshold for synaptic activation, a cell is either "inhibited" ($s_\infty(V_{\text{pre}}) = 1$) or "uninhibited" ($s_\infty(V_{\text{pre}}) = 0$), depending on whether the presynaptic cell's membrane potential is above or below η_{syn} (plotted as a vertical dotted line). Accordingly, the V-nullcline for a cell is either the lower N-shaped curve (the "inhibited" V-nullcline; the solid curve) or the upper N-shaped curve (the "uninhibited" V-nullcline; the dashed curve). Note that if uncoupled, the isolated cells would approach a depolarized steady state at $V_1 = 13$ mV, $n_1 = 0.85$, as indicated by the intersection between the n-nullcline and the uninhibited V-nullcline. Because the HCO is assumed to be a relaxation-like oscillator, dynamics in the V-direction are much faster than those in the n-direction. This implies that, if a cell is not near the V-nullcline, the state of the cell will quickly move to the corresponding stable branch of the V-nullcline (the branches with negative slopes). The evolution of cell 1's state that corresponds to the time series in Fig. 1 is plotted as a trajectory in phase space for a full period. Points along the trajectory (solid dots for the first half cycle and open circles for the second half) are plotted at equal time steps, thus the density of the points along the trajectory indicate the rates of change of the system. Note that, in both the release-type and the escape-type half-center oscillations, the density of points increases as the system moves along the right branch of the uninhibited V-nullcline and the left branch of the inhibited V-nullcline. This is the signature of the exponential deceleration of the cells' state as they slowly progress through the active state and the suppressed state. As suggested above, this deceleration plays a key role in determining the shapes of the PRCs. Cell 2's trajectory would be identical to cell 1's trajectory subject to a half-period phase shift.

In the following explanations, it is important to distinguish the effects of perturbations on the *state* of the cells in the (V, n) phase space and the effects on the *timing* of the release/escape processes. Also note that we use the term "state" not refer to the active or suppressed state but more specifically to the exact location of the cell in the (V, n) phase space.

3.2.1 Mechanisms shaping the PRCs of release-type HCOs

Under the release mechanism, the half-center oscillations are controlled by the termination of the synaptic inhibition to the suppressed cell (as described in Section 3.1 and in Wang and Rinzel 1992; Skinner et al. 1994; Daun et al. 2009). This suggests that the shape of the PRC of release-type HCOs can be understood by considering how perturbations ΔV lead to changes in timing Δt for the perturbed cell's membrane potential to drop below the synaptic threshold η_{syn}.

A $\rightarrow$ **B** : *Perturbations to cell 1 in the active state (phase* θ *from 0 to* $0.5T$*).* First consider the effect of a small brief positive perturbation ΔV delivered to cell 1 in the active state as it relaxes from the maximal membrane potential (point A) toward the synaptic threshold η_{syn} (point B) in the (V, n) phase plane (see schematic Fig. 5a top). The perturbation shifts the state of cell 1 and leads to a change in timing Δt for cell 1's membrane potential to reach the η_{syn}. As cell 1 progresses through the active state (A $\rightarrow$ B), the state of cell 1 moves upward closely adhering to the stable right branch of the uninhibited ($s_\infty = 0$) V-nullcline toward the n-nullcline (i.e., slow hyperpolarization and increase of n_1). Thus, the dynamics of cell 1 exponentially decelerate

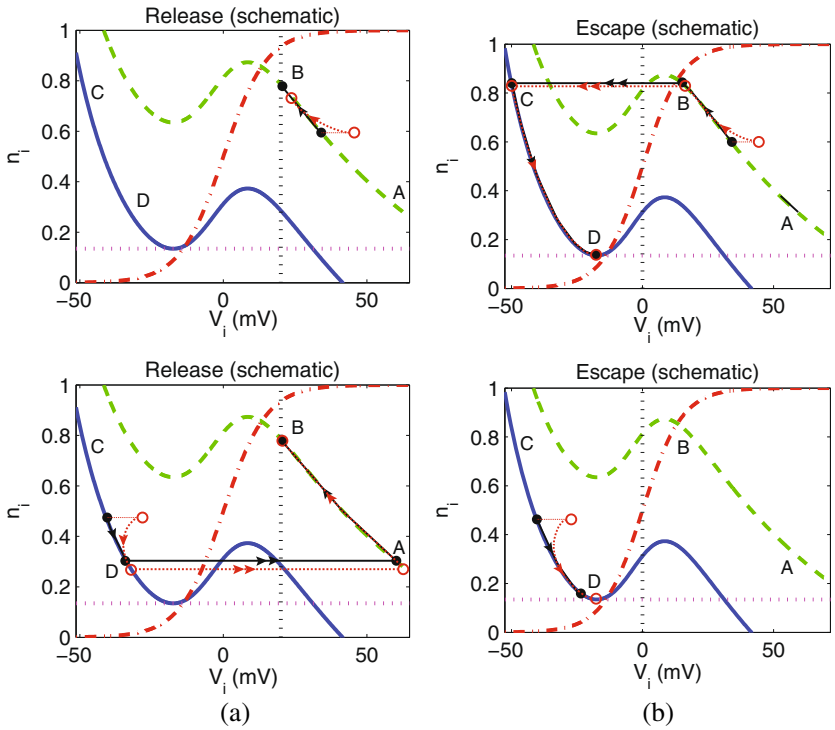

Fig. 5 Perturbations delivered to HCOs under different mechanisms and at different phases have fundamentally different effects on the HCO's phase shifts. The schematic dynamics of (**a**) a release-type HCO and (**b**) an escape-type HCO in the (V, n) phase plane. In both (**a**) and (**b**), the top figure shows the effect of a perturbation delivered to a cell in the active state, and the bottom figure shows the effect of a perturbation delivered to a cell in the suppressed state. The trajectories of the states of an unperturbed cell and a perturbed cell are plotted for comparison. The unperturbed cell is indicated by filled circles with a solid trajectory, and the perturbed cell is indicated by open circles with a dashed trajectory. The vertical dotted line indicates the synaptic threshold η_{syn}. The horizontal dotted line indicates the escape threshold n_{esc}. Markers A, B, C, D for cell 1 are used to indicate landmark points as in Fig. 4, which correspond to A, B, C, D in Figs. 1 and 2

as it approaches the stable steady state for the isolated cell, and there is a corresponding contraction of points in the (V, n) phase space around cell 1's trajectory (see A $\rightarrow$ B in Fig. 4a). This makes the timing of the HCO more sensitive to perturbations to cell 1 as it approaches η_{syn}; the magnitude of Δt in response to a perturbation ΔV will tend to increase exponentially as the timing of the perturbation occurs later in the active state. This implies that the magnitude of the first order PRC should increase significantly as θ approaches the phase at which cell 1's membrane potential reaches η_{syn}.

The mechanisms underlying this behavior are similar to those underlying the increased sensitivity of Morris-Lecar-type relaxation-oscillators as they approach the upper right knee of the V-nullcline in the "active" state (Izhikevich 2000; Coombes 2001; Rinzel and Ermentrout 1989). Timing delays are typical for Morris-Lecar-type relaxation-oscillators in response to perturbations at these phases, and therefore delays are expected for the Morris-Lecar-based HCO models in response to perturbations near the synaptic threshold. Indeed, perturbations delivered at times when the HCO system is very close to the threshold should cause delays because the positive perturbation pushes the active cell away from the threshold. Note however that there is no guarantee that perturbations delivered early in the active state will lead to delays (in the Morris-Lecar-based HCO model and the single cell Morris-Lecar-type relaxation-oscillator). Timing advances can sometimes occur due to the dynamical interactions between the change in the membrane potential V and the gating variable n. In any case, the timing shifts of the HCO due to perturbations to cells early in the active state will be relatively small due to the lack of sensitivity of the system at these states.

B $\rightarrow$ C : *Perturbations to cell 1 during the transition from the active state to the suppressed state (phase $\theta \sim 0.5T$).* Cell 1 eventually crosses the synaptic threshold η_{syn} shortly before phase $0.5T$. This turns off the synaptic input from cell 1 to cell 2. Cell 2 then rapidly depolarizes and turns on the inhibition to cell 1, which ultimately leads to the rapid hyperpolarization of cell 1 (B $\rightarrow$ C in Fig. 4a). Because voltage is changing rapidly during the transition from the active to the suppressed state, ΔV perturbations during this transition should have negligible effects.

C → D : *Perturbations to cell 1 in the suppressed state (phase θ from $0.5T$ to T).* Now consider the effects of perturbations ΔV to cell 1 in the suppressed state (schematic Fig. 5a bottom). At phase $\theta = 0.5T$, cell 1 is suppressed by inhibition from cell 2 and is at the minimal membrane potential (point C). As cell 1 progresses through the suppressed state, its state moves downward in the (V, n) phase plane along the stable left branch of the inhibited ($s_\infty = 1$) V-nullcline toward the n-nullcline (i.e., slow depolarization and decrease of n_1; C → D). Similar to the dynamics in the active state, the dynamics of cell 1 during the suppressed state exponentially decelerate, and there is a contraction of points in phase space around cell 1's trajectory (see C → D in Fig. 4a). When cell 1 is perturbed, the state of cell 1 will be altered, and in general there will be a shift in timing of cell 1 *within the suppressed state* (as shown in Fig. 5a bottom near D). However, this shift in timing of cell 1 is only transient. The perturbation to cell 1 does not affect the time at which cell 2 reaches the synaptic threshold and releases cell 1 from inhibition; this is controlled entirely by the intrinsic dynamics of the uninhibited cell 2. Furthermore, while the perturbation to cell 1 could in principle affect the time at which cell 1 reaches the synaptic threshold on the second half of the cycle and lead to a timing shift of the HCO Δt, this effect is negligible. Because of the contraction of points around cell 1's trajectory, the change in *state* of the suppressed cell 1 due to the perturbation, which was small immediately after the perturbation, gets even smaller before cell 1 is released from inhibition (see Fig. 5a). When cell 1 jumps to the active state, the magnitude of the change in *state* due to the perturbation is preserved and therefore remains very small. As explained above, cells at the beginning of the active state are insensitive to small changes in the *state*. Thus, perturbations' effect on the timing change Δt for cell 1 to reach η_{syn} will be insignificant, and the first-order PRC of the HCO should be close to zero for phases $0.5T$ to T.

D → A : *Perturbations to cell 1 during the transition from the suppressed state to the active state (phase $\theta \sim T$).* When cell 2 crosses η_{syn}, it releases cell 1 from inhibition and cell 1 rapidly depolarizes (D → A in Fig. 4a). As was the case for the active to suppressed state transition, the effects of perturbations during this fast transition will be negligible. At phase $\theta = T$, cell 1 returns to the initial active state (point A in Fig. 4a), and the cycle begins again.

The thick solid curve in Fig. 6a plots the first order PRC of the release-type HCO, demonstrating that it takes the shape described above. In addition, Fig. 6a shows that the first order PRC of the release-type HCO is indistinguishable from its asymptotic PRC (the thin dashed curve). This illustrates that the timing shifts due to the perturbation are essentially complete within a single cycle, and that the mechanisms shaping the asymptotic PRC are those that shape the first order PRC as described above. Why are there no substantial higher order effects of the perturbation on the changes in transition times Δt (i.e., why are the first-order PRC and the asymptotic PRC virtually identical)? A perturbation to cell 1 in the suppressed phase has little effect on the first full cycle and therefore cannot have any substantial effect on the following cycles. A perturbation to cell 1 when it is in the active state alters the time at which the suppressed cell 2 is released from inhibition and therefore alters the *state* of the cell 2 when it is released. However, because the dynamics are relatively slow near the end of the suppressed state, this change in state of cell 2 will be small. This in turn implies that change in state of cell 2 at the beginning of active state will be small. As mentioned above, because dynamics are relatively fast at the beginning of the active state, this change in state of cell 2 will have very little effect on the *time* at which it reaches threshold and releases cell 1. Thus, any subsequent changes in timing will be negligible.

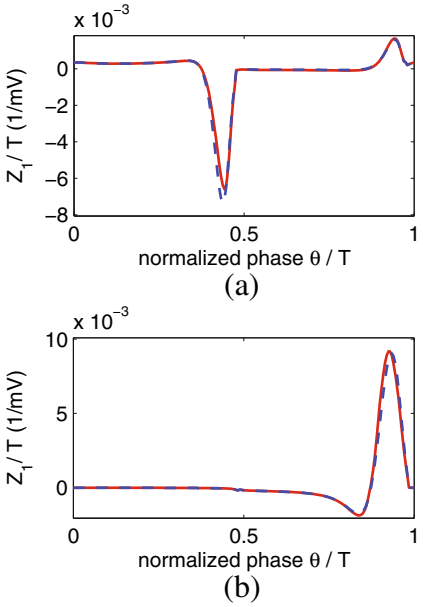

Fig. 6 The first order PRCs of (**a**) a release-type HCO and (**b**) an escape-type HCO (*thick solid curves*). The thin dashed curve represents the (infinitesimal) PRC calculated using the adjoint method. Note that the first order PRC and the PRC are virtually indistinguishable

Summary for release-type HCOs The timing of a release-type HCO is controlled by the event that the active cell's membrane potential falls below the synaptic threshold. Therefore, if the active cell is perturbed, the change in its timing will directly translate into the phase shift of the HCO,

and thus the phase response properties of the HCO is inherited from the active cell's dynamics. Because dynamics of the cells undergo exponential deceleration during the active state, cells are relatively insensitive to perturbations early in the active state and respond with exponentially growing delays as the active phase progresses. On the other hand, if the suppressed cell is perturbed, any change in its timing will be nullified when the cell jumps to the active state due to the exponential deceleration of the dynamics in the suppressed state and the insensitivity of the HCO to perturbations to cells at the beginning of the active state. This implies that the PRCs for release-type HCOs are dominated by a negative peak late in the first half of the cycle followed by a portion with insignificant phase shifts in the second half of the cycle.

3.2.2 Mechanisms shaping the PRCs of escape-type HCOs

A similar analysis can be used to uncover the mechanisms shaping the PRCs for escape-type HCOs. In fact, by noting (1) the similarities between dynamics of the escape and release mechanisms in phase space (i.e., the same nullcline structure and the exponential deceleration of the cells' states during the active and suppressed states) and (2) that the escape threshold n_{esc} plays the role that the synaptic threshold η_{syn} played in the release mechanism, we expect that very similar mechanisms are at work.

C $\rightarrow$ **D** : *Perturbations to cell 1 in the suppressed state (phase θ from $0.5T$ to T)* First consider the effect of a small brief positive perturbation ΔV on the inhibited suppressed cell 1 during phases θ from $0.5T$ to T (see schematic Fig. 5b bottom). At phase $\theta = 0.5T$, cell 1 is suppressed by inhibition from cell 2 and has a minimum membrane potential (point C). The perturbation will shift the state of cell 1 and lead to a change in timing Δt for cell 1 to reach the escape threshold n_{esc} (point D). As cell 1 progresses through the suppressed state in the (V, n) phase plane, it moves slowly downward along the stable left branch of the inhibited V-nullcline toward the lower left knee of this nullcline (C $\rightarrow$ D), and there is a contraction of points in phase space around the suppressed cell 1's trajectory (see Fig. 4b). Thus, the timing of the HCO becomes more sensitive to perturbations to cell 1 as its state approaches the lower left knee of the inhibited V-nullcline, reaching a maximal sensitivity around the knee. The typical response properties of single-cell Morris-Lecar oscillators suggest that timing advances should arise for the escape-type HCO in response to perturbations near the lower knee of the left branch of the inhibited V-nullcline. This implies that the first order PRC should increase as cell 1 progresses through the suppressed state, reaching a maximum near $\theta \sim T$.

D $\rightarrow$ **A** : *Perturbations to cell 1 during the transition from the suppressed state to the active state (phase $\theta \sim T$).* Immediately before phase $\theta = T$, cell 1 reaches the lower left knee of the inhibited V-nullcline. This ultimately leads to the rapid transition of cell 1 from the suppressed state to the active state. Perturbations delivered during this fast transition will have negligible effects.

A $\rightarrow$ **B** : *Perturbations to cell 1 in the active state (phase θ from 0 to $0.5T$).* Now consider the effects of perturbations ΔV to cell 1 in the active state (schematic Fig. 5b top). At phase $\theta = 0$, cell 1 is active, uninhibited and has a maximal membrane potential (point A). As described for the release case, as cell 1 progresses through its active state in the (V, n) phase plane, it approaches a steady state for the isolated cell, and there is a contraction of points in phase space around cell 1's trajectory. However, in the escape mechanism, cell 1 does not make a transition to the suppressed state until the suppressed cell 2 escapes from inhibition. Because cell 1 approaches a steady state, the changes in the active cell's *state* due to perturbations will exponentially decrease as the cell progresses through the active state. Therefore, when the cell eventually jumps to the suppressed state, any changes in the cell's state due to perturbations will be very small. Because cells are insensitive to changes in state at the beginning of the suppressed state, the small change in cell 1's state due to the perturbation will have an insignificant effect on the change in time Δt for the cell to reach the lower left knee of the inhibited V-nullcline. This implies that the first-order PRC of the HCO should be close to zero for phases from 0 to $0.5T$.

B $\rightarrow$ **C** : *Perturbations to cell 1 during the transition from the active state to the suppressed state (phase $\theta \sim 0.5T$).* As cell 2 escapes from inhibition and turns on the inhibition to cell 1, cell 1 rapidly jumps to the stable left branch of the inhibited V-nullcline. The rapid changes in voltage ensure that the effects on Δt from perturbations ΔV delivered during this fast transition are negligible. At phase $\theta = 0.5T$, cell 1 returns to the state with a minimal membrane potential (point C).

Figure 6b shows that the first order PRC (the thick solid curve) matches the shape of the PRC (the thin dashed curve), i.e., there are no higher order effects. The explanation for the lack of higher order effects of perturbations on the changes in timing Δt for the escape case is very similar to that for the release case.

Summary for escape-type HCOs The timing of an escape-type HCO is controlled by the event that the suppressed cell's gating variable falls below the escape threshold. Therefore, if the suppressed cell is perturbed, the change in its timing will directly translate into the phase shift of the HCO, and thus the phase response properties of the HCO is inherited from the suppressed cell's dynamics. Because

dynamics of the cells undergo exponential deceleration during the suppressed state, cells are relatively insensitive to perturbations early in the suppressed state and respond with exponentially growing advances as the suppressed phase progresses. On the other hand, if the active cell is perturbed, any change in its timing will be nullified when the cell jumps to the suppressed state due to the exponential deceleration of the dynamics in the active state and the insensitivity of the HCO to perturbations to cells at the beginning of the suppressed state. This implies that the PRCs for escape-type HCOs will be dominated by a positive peak in the second half of the cycle preceded by a portion with insignificant phase shifts in the first half of the cycle.

3.3 Half-center oscillations involving both release and escape mechanisms

In the previous subsections, half-center oscillations were described as being generated by either the release or escape mechanism. However, not every HCO can be classified as being distinctly release-type or escape-type. In fact, continuous changes in parameters can lead to smooth transition between release and escape (Shpiro et al. 2007). Thus, dynamics of an HCO may involve elements from both the release and escape mechanisms, and therefore the PRC of an HCO may have both a negative peak late in the first half of the cycle and a positive peak late in the second half of the cycle. Nevertheless, the explanations presented in Section 3.2 can still be used to understand shapes of PRCs for these less distinct cases.

The PRCs of release-type HCOs in Fig. 3b and c show that, when the synaptic activation curve is less steep (larger k_{syn}), the large negative peak late in the first half of the cycle persists, but the small escape-like positive peak late in the second half of the cycle increases in size. If the synaptic threshold is infinitely sharp ($k_{\text{syn}} \approx 0$), then the synaptic inhibition was either fully on ($s_\infty = 1$) or fully off ($s_\infty = 0$). However, with a larger k_{syn}, the level of synaptic inhibition changes smoothly with the presynaptic membrane potential (i.e., η_{syn} can no longer be thought of as an all-or-none "threshold"). This leads to a gradual increase in the escape threshold n_{esc} during the waning of the inhibition. In the (V, n) phase plane, this gradual increase in n_{esc} during the release process corresponds to the lower left knee of the inhibited V-nullcline continuously shifting upward toward the uninhibited V-nullcline (see the online supplemental material for animated phase plane movies). Compared to the idealized case where the suppressed cell cannot reach the lower left knee of its V-nullcline because the knee is too low (see Fig. 5a bottom and descriptions in Section 3.2.1 for **C** $\rightarrow$ **D**), in the case where the synaptic activation is smoother, the lower left knee gradually rises during the release process and becomes within the reach of the suppressed cell. In this scenario, perturbations to the suppressed cell could have timing shifts similar to those in escape-type HCOs (see Fig. 5b bottom and descriptions in Section 3.2.2 for **C** $\rightarrow$ **D**). Therefore, brief positive perturbations delivered to the suppressed cell just before it escapes can have a significant phase advancing effect on the full HCO, and hence lead to the escape-like positive peak (late in the second half of the cycle) in addition to the large negative peak (late in the first half of the cycle).

Parameters other than k_{syn} can also affect the oscillation mechanism underlying an HCO and hence the shape of its PRC. As an example, Fig. 7a depicts the PRCs of an HCO with a varying bias current in both cells in the HCO, I. As I increases, there is a smooth transition from release to escape. Initially at $I = 0.85\ \mu\text{A/cm}^2$, the PRC has a dominant negative peak late in the first half of period, which is the signature of the release mechanism. As I increases, the HCO and its PRC become less release-like and more escape-like. That is, the large negative peak becomes smaller, while a positive peak late in the second half of the period develops and grows larger. At an intermediate value $I = 0.95\ \mu\text{A/cm}^2$, the PRC's positive and negative peaks are approximately equal in size, which implies that the two mechanisms play equally weighted roles in generating phase response properties. As I further increases to $I = 1.05\ \mu\text{A/cm}^2$, the HCO becomes distinctly escape-type with a dominant positive peak late in the second half of the period. The transition from release to escape is reflected in the average of the PRC over a period ($\langle Z \rangle = \frac{1}{T}\int_0^T Z(\theta)d\theta$), which is plotted as a function of I in Fig. 7b (solid curve, normalized by the period T). As I increases, $\langle Z \rangle$ smoothly increases from a negative value reflecting the dominant negative peak in release-type HCOs' PRCs to a positive value reflecting the dominant positive peak in escape-type HCOs' PRCs.

3.4 Applications of PRCs

3.4.1 Effects of changes in bias currents on the frequency of half-center oscillations

Figure 7b shows that the frequency vs. bias current (f-I) curve of the HCO is non-monotonic. When the HCO exhibits release-type behavior at lower values of I, f decreases with I; when the HCO exhibits escape-type behavior at higher values of I, f increases with I. This dependence of the f-I curve of HCOs on the mechanism of oscillation was pointed out in Shpiro et al. (2007), Curtu et al. (2008) and Daun et al. (2009).

The link between the HCO mechanism and the frequency dependence on the bias currents can be readily understood

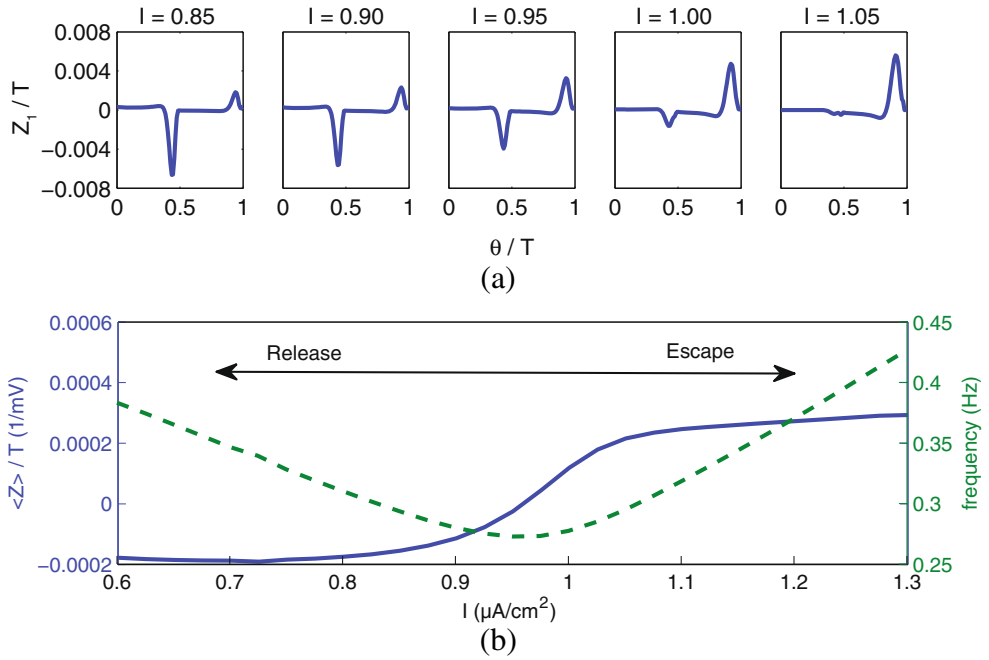

Fig. 7 The link between the PRC and the f-I curve. **a** The PRCs of HCOs with different values of the bias current to both cells. As I increases, there is a smooth transition from a release-type PRC to an escape-type PRC. **b** Average of the PRC and frequency of oscillation as functions of I. Solid curve: the average of the PRC over a period, denoted by $\langle Z\rangle$, normalized by T. When the PRC has a dominant negative peak, which is a signature of the release mechanism, $\langle Z\rangle$ is negative; whereas when the PRC has a dominant negative peak, which is a signature of the release mechanism, $\langle Z\rangle$ is positive. Dashed curve: the frequency of the half-center oscillations (f). f decreases when $\langle Z\rangle < 0$, and increases when $\langle Z\rangle > 0$

in terms of the PRCs. According to the phase model for the HCO (Eq. (8) in Section 2.3), $\frac{1}{T}\frac{d\phi}{dt}$, and therefore $\frac{1}{T}H(\phi)$, is the change in instantaneous frequency of an oscillator that results from the perturbation I_{ext}. If the perturbation is taken to be a small constant change in the bias current in both cells of the HCO (i.e., $I_{\text{ext},i} = \Delta I$, $i = 1, 2$), then the change in HCO's frequency is

$$\Delta f = \frac{1}{T}H(\phi) = \frac{1}{T}\sum_{i=1}^{2}\frac{1}{T}\int_0^T Z_i(s+\phi)\frac{\Delta I}{C}ds$$
$$= \frac{2}{CT}\langle Z\rangle\Delta I.$$

Taking the limit $\Delta I \to 0$, we see that

$$\frac{df}{dI} = \left(\frac{2}{CT}\right)\langle Z\rangle. \tag{9}$$

That is, the instantaneous slope of the HCO's f-I curve is proportional to the average value of the PRC $\langle Z\rangle$ (Schwemmer and Lewis 2011). This relationship links the f-I curves, the PRCs and the oscillation mechanisms of HCOs. A release-type HCO has a negative average value of its PRC, which leads to the negative slope in the f-I curve; whereas an escape-type HCO has a positive average value of its PRC, which leads to a positive slope in the f-I curve.

3.4.2 The phase-locking property of a forced HCO

Given a particular PRC $Z(\theta)$, the phase model Eq. (8) can be used to determine the phase-locking property of an HCO forced by a T-periodic external input. Here, we demonstrate that release-type HCOs and escape-type HCOs support very different phase-locking dynamics. Figure 8a plots the functions $H(\phi)$ for both the release-type HCO and the escape-type HCO (as defined in Fig. 1a and 1b, respectively) when cell 1 is subject to a weak periodic inhibitory input. The input to cell 1 is $I_{\text{ext},1}(t) = -\epsilon\mathcal{H}\big((t \bmod T) - 0.25T\big)$, where $\mathcal{H}$ is the Heaviside function and ϵ is the strength of the forcing. Recall that the zero crossings of $H(\phi)$ with negative slope correspond to the stable phase-locked states. We see that the release-type HCO is stably phase-locked to the periodic input I_{ext} with a 19 %-period advance relative to the stimulus, whereas the escape-type HCO is stably phase-locked to I_{ext} with a 7 %-period phase delay.

Figure 8b shows how the T-periodically forced HCO's phase-locked states change as the bias current I changes. The solid curve plots the stable phase-locked states (zero crossings of H with a negative slope), and the dashed curve plots the unstable phase-locked states (zero crossings with a positive slope). At low values of bias current ($I \sim 0.6\ \mu\text{A/cm}^2$), the HCO has one stable phase-locked

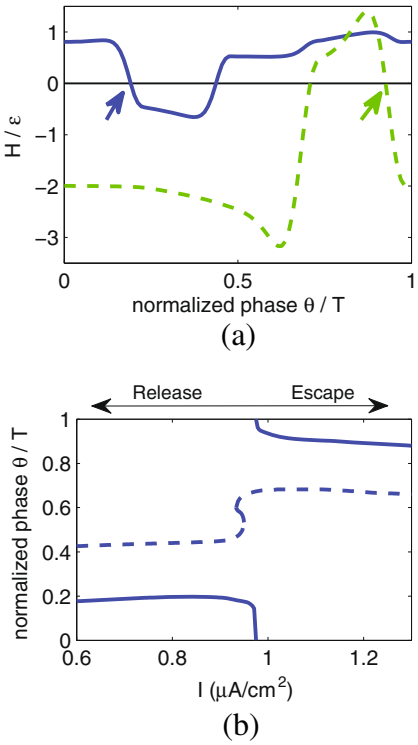

Fig. 8 Phase-locking of HCOs to periodic input. **a** The interaction functions H for two HCOs subjected to periodic forcing to cell 1. *Solid curve:* H function for the release-type HCO (from Fig. 1a). *Dashed curve:* H function for the escape-type HCO (from Fig. 1b). The arrow on the left points to the stable phase-locked state (at $0.19T$) of the release-type HCO, and the arrow on the right points to the stable phase-locked state (at $0.93T$ or $-0.07T$) of the escape-type HCO. **b** The phase-locked states of periodically forced HCOs with different values of the bias current to both cells I (bifurcation diagram). *Solid curve:* the stable phase-locked states with different values of I. *Dashed curve:* unstable phase-locked states at different values of I. Parameters are the same as those in (a) except that I is varied

state around 20 %-period and one unstable phase-locked state around 40 %-period. As I increases, the stable phase-locked state remains around 20 %-period until I reaches $\sim$0.97 μA/cm^2, at which point the stable phase-locked state quickly changes to approximately 90 %-period. Around this point, a pair of saddle node bifurcation associated with the unstable phase-locked state leads to region of bistability, but this bistability only exists for a very narrow range of I. It is important to note that the critical region in parameter space around $I \sim 0.97$ μA/cm^2 corresponds to the HCO's transition from release to escape: when below $I \sim 0.97$ μA/cm^2, the HCO is release-dominated (as illustrated in Fig. 7b), and a stable phase-locked state exists at around 20 %-period; whereas when above $I \sim 0.97$ μA/cm^2, the HCO is escape-dominated, and a stable phase-locked state exists at around 90 %-period. This shows that different half-center oscillation mechanisms can lead to strikingly different phase-locked states for forced HCOs.

4 Discussion

A phase response curve (PRC) describes the phase shifts of an oscillator as a function of the phase at which a perturbation is given in an oscillation cycle. In neuroscience, PRCs are widely used to quantify the response properties of neural oscillators and predict phase-locking in neural systems. Typically, each neural oscillator is viewed as an intrinsically oscillatory neuron, and hence PRCs are usually computed for single cells. However, oscillations in neural systems often arise from network interactions, as in the case of half-center oscillators (HCOs). Despite this fact, there have been few theoretical studies that analyze the phase response properties of network-based oscillators.

In this manuscript, we examine the phase response properties of HCOs that consist of two non-oscillatory Morris-Lecar cells connected by fast inhibitory synapses. By analyzing the phase space structure of Morris-Lecar-type HCO models, we show how the two basic mechanisms for half-center oscillations, "release" and "escape", lead to strikingly different phase response properties. The timing of an HCO is controlled by a trigger event that switches the direction of inhibition between the two cells and leads to the transition of the cells between the active and suppressed states. When the HCO is not undergoing transition, only one of the cells in the HCO is in control of the timing of the system. If the cell in control of the trigger event is perturbed, the change in timing of this cell will directly translate into the phase shift of the HCO. If the other cell is perturbed, any transient change in timing of this cell will be eliminated when the cell makes the next transition. This is due to the exponential deceleration of the cell's dynamics before its transition and the initial insensitivity of the HCO to perturbations delivered to a cell soon after its transition. The trigger event of a release-type HCO occurs when the active cell's membrane potential falls below the synaptic threshold. Therefore, the effects of perturbations delivered to the active cell will be manifested in the PRC by a large negative peak (delay) late in the active phase, whereas perturbations delivered to the suppressed cell will not lead to significant phase shifts. On the other hand, the trigger event of an escape-type HCO occurs when the suppressed cell's gating variable drops below the escape threshold. Therefore, the effects of perturbations delivered to the suppressed cell will be manifested in a dominant advance portion of the PRC late in the suppressed phase, whereas perturbations delivered to the active cell will not lead to significant phase shifts. Note that, given the structure of the Morris-Lecar-type HCO model considered here (i.e., fast synapses and relaxation-like dynamics), not only do the release and escape mechanisms determine the shape of the HCOs' PRCs, the shape of an HCO's PRC can also be used to determine the HCO's underlying mechanism.

For our analysis, we place some idealizations on the Morris-Lecar-type HCO model (Skinner et al. 1994): ϵ_n is relatively small, i.e., the HCO has a relaxation-oscillator-like dynamics, and k_{syn} is small, i.e., the synaptic activation is steep. Despite these idealizations, the qualitative aspects of our results hold for larger ϵ_n and/or k_{syn}. As illustrated in Fig. 3, the basic shape of the PRC is unchanged with small changes in ϵ_n and k_{syn}. In general, if HCOs have a less relaxation-oscillator-like dynamics (i.e., a larger ϵ_n), their PRCs will be smoother and less peaked. On the other hand, less steep thresholds for the synaptic activation (i.e., a larger k_{syn}) will lead to HCOs in which both the release and escape mechanisms contribute to their half-center oscillation, and therefore PRCs will have both a negative peak late in the active phase and a positive peak late in the suppressed phase.

It is important to note that even though changes in biophysical parameters can lead to changes in the shape of the HCO's PRC, the link between the PRC's shape and the HCO's mechanism is unchanged. For example, by increasing k_{syn}, the boundary between the release and escape mechanisms blurs. Nevertheless, a negative peak late in the first half of the cycle of the PRC indicates the existence of a release mechanism (i.e., the timing of the cells' transition between the active and suppressed states is sensitive to perturbations delivered to the active cell late in the first half of the cycle), and a positive peak late in the second half of the cycle of the PRC indicates the existence of an escape mechanism (i.e., the timing of the cells' transition is sensitive to perturbations delivered to the suppressed cell late in the second half of the cycle).

As Skinner et al. (1994), LoFaro et al. (1994) and Rowat and Selverston (1993) demonstrated, the release and escape mechanisms of HCOs can be generated by several different ionic mechanisms. Wang and Rinzel (1992) first characterized the release and escape mechanisms based on a minimal ionic model in which the oscillations are driven by a post-inhibitory rebound current. Skinner et al. (1994) refined and generalized Wang and Rinzel's results using a Morris-Lecar-based model (as we used here) to explore cases where the cells are either intrinsically quiescent or intrinsically oscillatory. Daun et al. (2009) studied three different HCO models based on different ionic currents: a slowly inactivating persistent sodium current, a slowly activating calcium-dependent potassium current and a post-inhibitory rebound current. Although the underlying biophysical mechanisms were different, the dynamical mechanisms for these models are all based on fast-slow cellular (relaxation-oscillator-like) dynamics similar to the Morris-Lecar-based model with fast inhibitory synapses. In fact, Rowat and Selverston (1997) further demonstrated that the release and escape mechanisms are sufficient to produce oscillatory behavior in all cases of reciprocal inhibition in an HCO model where each cell is modeled by a 2-dimensional fast-slow system with fast synaptic coupling. This suggests that our basic results on how the release and escape mechanisms shape the HCO's PRC can apply to a wide variety of HCOs models that share similar dynamical properties. Note that this family of models also includes population or competition models such as the binocular rivalry models examined in Shpiro et al. (2007), Curtu et al. (2008) and Seely and Chow (2011) and the spike-rate-based CPG model in Varkonyi et al. (2008). Indeed, in Appendix A and B, we show that the PRCs for Morris-Lecar-based HCOs with intrinsically oscillatory cells (Skinner et al. 1994) and the Wang-Rinzel model for the release and escape mechanisms have the same basic shapes as those described here.

Ko and Ermentrout (2009) and Schlichter (2011) previously studied how the PRCs of HCOs, which were modeled by two weakly coupled phase oscillators, were shaped by the PRCs of the individual oscillators. Our work fundamentally differs from this previous work in that we considered an HCO consisting of two conductance-based model neurons that are strongly coupled. Nadim et al. (2011) modeled an HCO in the crustacean pyloric circuit by using a single intrinsically oscillatory Morris-Lecar-type neuron with delayed inhibitory feedback. They showed the delayed inhibitory feedback decreased the overall magnitude of the oscillator's PRC, and therefore promoted the stability of the oscillation. This suggests that the HCO circuit structure may promote stable oscillations. Similar to the analysis in Section 3.2, Nadim et al. used phase plane arguments to show that the delayed inhibition sped up the dynamics of the system at particular phases, making the system less sensitive to perturbations at these phases. This mechanism for shaping PRCs appears to be different than the mechanisms that we described for our HCO model. This difference is likely due to the different modeling assumptions, e.g., single-cell model vs. two-cell model, smoother dynamics vs. relaxation-oscillator-like dynamics. More work is required to coherently link these two PRC-shaping mechanisms suggested by the two different models.

Our idealized model does not include many biophysical features of real HCOs or biophysically detailed HCO models, such as fast spiking dynamics, heterogeneity of cells and more realistic synaptic dynamics. Clewley (2011) computed the first and second order PRCs for a 38-dimensional leech heart HCO model consisting of two mutually coupled single-compartment cells with fast spiking dynamics during the cells' active state. Many aspects of the PRCs of the detailed model agree with our findings for the Morris-Lecar-based HCO model. Specifically, the PRCs of the detailed model showed an insensitivity of the HCO to perturbations at initial phases of both the active and suppressed states, and sometimes a high sensitivity near the end of the active

and/or suppressed states. Furthermore, some PRCs of the detailed model had shapes consistent with the release-type delays and escape-type advances. On the other hand, the detailed model's PRCs sometimes had bi-phasic or multi-phasic responses in the sensitive phases and high-frequency oscillations throughout the cycle (seemingly uncorrelated with the fast spikes). This suggests the detailed model has more complicated phase response properties than the Morris-Lecar-based model. We note, however, that the second order PRCs of the detailed model closely resemble the first order PRCs, indicating there are minimal higher order effects, as is the case in our Morris-Lecar-based model.

Nadim et al. (2011) measured a PRC for the central pattern generator (CPG) of the crustacean pyloric circuit, and Smarandache et al. (2009) measured the CPG underlying a segment of the crayfish swimmeret system. Both of these circuits are composed, at least partially, of HCO structures. The PRC for the pyloric CPG circuit showed increased sensitivity during the suppressed state and near the beginning of the transition to the active state, exhibiting a large escape-type advancing portion. The system also showed a small release-type delaying portion of the PRC. However, the PRC was much smoother than the PRCs for our Morris-Lecar-based HCO model. This is likely due to smoother dynamics in the pyloric rhythm generating circuit (i.e., less relaxation-oscillator-like dynamics) and possibly the longer stimulus duration used in generating the pyloric PRC. The PRC of the crayfish swimmeret system CPG showed both a large delaying portion during the active state and a large advancing portion during the suppressed state, and they were even smoother than the pyloric PRC. Again, this smoothness is at least partially due to the long stimulus (about 40 % of the period) used to obtain the swimmeret PRC, and it could also be due to the fact that the swimmeret CPG was indirectly stimulated through a coordinating interneuron. The similarities between these experimentally measured PRCs and the PRCs of the Morris-Lecar-type HCO models suggest that both the pyloric and the swimmeret CPGs' oscillations involve both the release and the escape mechanisms, as described in Sections 3.2 and 3.3. However, more evidence is needed to strengthen this hypothesis. For instance, the influence of modulating the CPG dynamics on the PRCs' shape could be examined. The phase space structure of the Morris-Lecar-based model predicts that pharmacologically depolarizing the cells or partially blocking the synaptic inhibition should promote escape-type dynamics, and thus would lead to a larger positive bump at phases late in the active state, e.g., see Fig. 7.

Despite the generality of our results, there are still several caveats and open questions that need to be pointed out. (i) Models that we consider, e.g., the Morris-Lecar-based HCO model (Skinner et al. 1994) and the Wang-Rinzel model (Wang and Rinzel 1992), only describe the envelop of bursts or non-bursting dynamics. Explicitly including spikes in a bursting model will result in more complicated phase response properties (Sherwood and Guckenheimer 2010). Some of the basic PRC properties appear to persist in biophysically detailed models that include bursting dynamics (Clewley 2011). However, a better understanding of the similarities and differences in the idealized and the detailed models is necessary. (ii) The two neurons in our HCO model are assumed to be identical. If the heterogeneity between the two neurons is sufficiently small, the shape of the PRC will be similar to the case for the HCO with identical neurons. If the heterogeneity is large, then the PRC may be different. However, the PRC's shape may still be understood based on the ideas presented in this article. (iii) The synaptic connections in our HCO model are simulated by using the fast threshold modulation model. Although this instantaneous synapse model can be a good approximation to sufficiently fast synapses, it cannot capture the dynamics arising from slower synapses (Schlichter 2011; Clewley 2011). Furthermore, incorporating synaptic plasticity (for example, the central pattern generator (CPG) model with synaptic depression studied by Taylor et al. (2002) may further complicate the half-center oscillation mechanisms and the shape of the PRCs. (iv) Our HCO model consists of two neurons coupled by mutual inhibition. However, many biological CPGs contain more than two populations of neurons (Grillner 2003; Kiehn 2006; Kristan et al. 2005; Varkonyi et al. 2008; Smith et al. 2007). A different analysis may be required to study the phase response properties of these CPGs. Nevertheless, because half-center structure is integral to many CPGs, we expect that some of our results of HCOs will carry over to these more complicated CPGs.

Acknowledgments This work was supported by the National Science Foundation under the grant CRCNS 0905063. The authors would like to thank Brian Mulloney, Lucy Spardy and Michael Schwemmer for their careful reading of the manuscript and helpful comments.

Appendix A: PRCs under the "intrinsic release" and "synaptic release" mechanisms for the Morris-Lecar-based HCO model

Skinner et al. (1994) used a Morris-Lecar-based HCO model to show that the release and escape mechanisms can be further categorized into "intrinsic release", "synaptic release", "intrinsic escape" and "synaptic escape", depending on whether the cells' transitions between the active and suppressed states are due to synaptic dynamics or cells' intrinsic dynamics. Synaptic and intrinsic mechanisms can lead to different biophysical properties of HCOs. For example, in the synaptic release mechanism, the frequency of oscillation is sensitive to the synaptic threshold (η_{syn}),

whereas in the intrinsic release mechanism, the frequency is robust against changes in the synaptic threshold. In the cases presented in the main text, the release-type HCOs are under the synaptic release mechanism and the escape-type HCOs are under the intrinsic escape mechanism, as in Wang and Rinzel (1992).

Using arguments similar to those in Section 3.2, it can be readily shown that the PRCs for both the synaptic and intrinsic release mechanisms have the same basic characteristics, and the same for the escape case. Parameters used in our Morris-Lecar-based HCO model in the main text correspond to the synaptic release and the intrinsic escape mechanisms, where the cells are not intrinsic oscillators. Figures 9 and 10 show the PRCs of the Morris-Lecar-based HCOs under the intrinsic release mechanism and the synaptic escape mechanism, respectively, as defined in Skinner et al. (1994). Despite the biophysical differences between the intrinsic and synaptic mechanisms, both intrinsic and synaptic release-type HCOs have PRCs with a dominant negative peak late in the first half of the cycle (compare Fig. 9 with Fig. 2a), whereas both intrinsic and synaptic escape-type HCOs have PRCs with a dominant positive peak late in the second half of the cycle (compare Fig. 2b with Fig. 10).

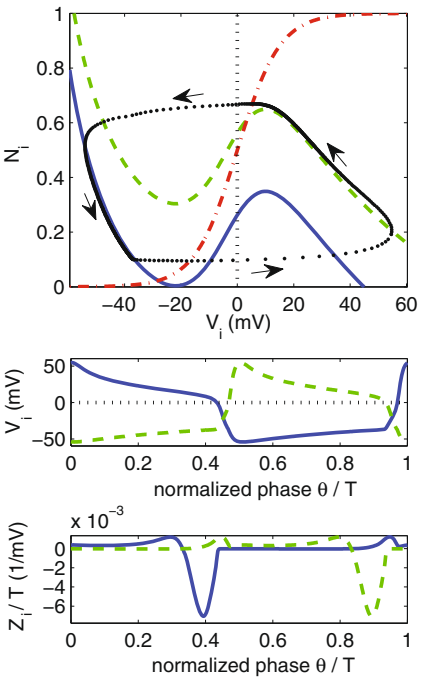

Fig. 9 Dynamics and the PRC of a Morris-Lecar-based HCO under the intrinsic release mechanism. $g_{syn} = 0.006$ mS/cm^2, $\eta_{syn} = 0$ mV and $I = 0.4$ μA/cm^2. *Top figure*: (V, n) phase plane. *Solid curve*: the V-nullcline when a cell is fully inhibited. *Dashed curve*: the V-nullcline when a cell is fully uninhibited. *Dash-dotted curve*: the n-nullcline, which is not dependent on the status of the presynaptic cell. *Dots*: cell 1's (or cell 2's) trajectory evenly spaced in time for a full cycle. The vertical dotted line indicates the synaptic threshold η_{syn}. *Middle figure*: membrane potential V_i of cell 1 (*solid curve*) and cell 2 (*dashed curve*) as functions of the phase (normalized by the period T). The horizontal dotted line is η_{syn}. *Bottom figure*: the PRCs of cell 1 (*solid curve*) and cell 2 (*dashed curve*). In the intrinsic release mechanism, the active cell's membrane potential is always above the synaptic threshold. The transition between the active and the suppressed states is triggered by the active cell's intrinsic properties

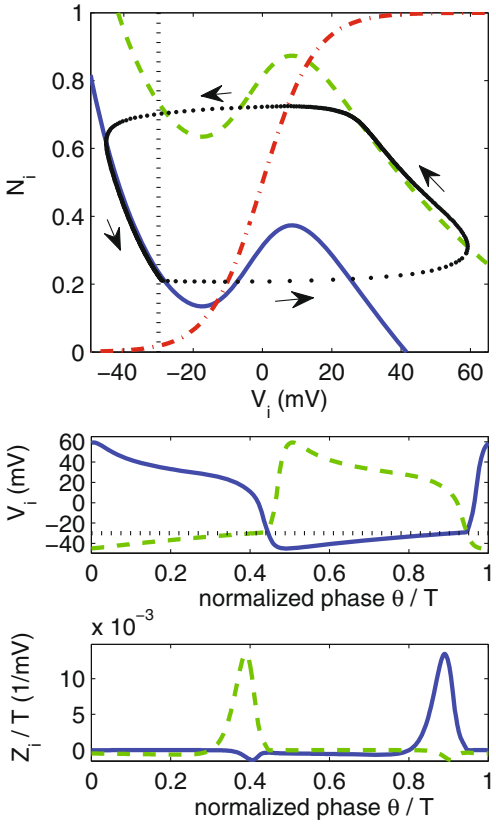

Fig. 10 Dynamics and the PRC of a Morris-Lecar-based HCO under the synaptic escape mechanism. $\eta_{syn} = -30$ mV. Same notations as in Fig. 9. In the synaptic escape mechanism, the transition between the active and the suppressed states is triggered by the suppressed cell's membrane potential rising above the synaptic threshold, and hence turning on the inhibition to the active cell

Appendix B: PRCs for the Wang-Rinzel (HCO) model

Wang and Rinzel (1992) described the release and escape mechanisms in a minimal ionic model for half-center oscillations involving a post-inhibitory rebound current. Figures 11 and 12 show the PRCs for the Wang-Rinzel model under the release and the escape mechanisms, respectively. As argued in the discussion section, the basic results of our work do not specifically rely on a particular choice of models. HCOs modeled using the Wang-Rinzel model have the same basic dynamics in terms of their phase portraits as the Morris-Lecar-type HCO models. Therefore, they have the same basic phase response properties as the HCO model

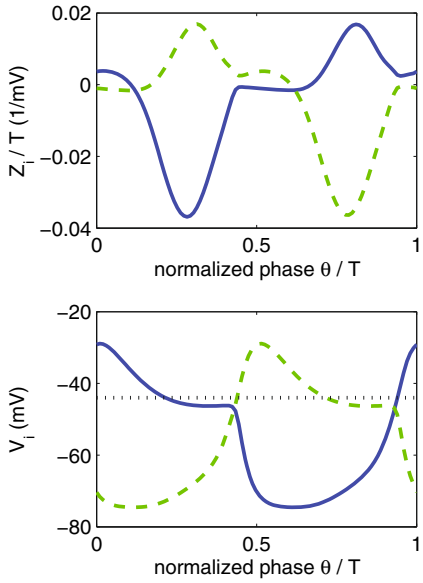

Fig. 11 The PRC of an HCO under the release mechanism using the Wang-Rinzel model. Same parameters as defined by Wang and Rinzel (1992). *Top figure*: The PRCs of cell 1 (*solid curve*) and cell 2 (*dashed curve*). *Bottom figure*: Membrane potential V_i of cell 1 (*solid curve*) and cell 2 (*dashed curve*) as functions of the phase (normalized by the period T). The horizontal dotted line is the synaptic threshold (η_{syn} as defined in Wang and Rinzel (1992))

in our article (compare Fig. 11 with Fig. 2a for the release mechanism, and compare Fig. 12 with Fig. 2b for the escape mechanism).

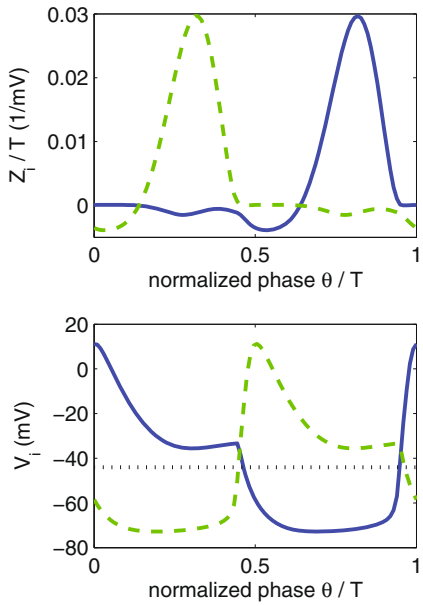

Fig. 12 The PRC of an HCO under the escape mechanism using the Wang-Rinzel model. Same parameters as defined by Wang and Rinzel (1992). Same notations as in Fig. 11

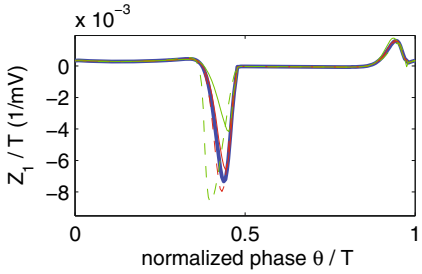

Fig. 13 The effects of perturbation strength on the PRC of a release-type HCO. The thickest solid line is the infinitesimal PRC as shown in Fig. 2a. The thinner solid lines are the PRCs computed using delta function stimuli resulting in 1 mV and 5 mV perturbations. The thinner dashed lines are the PRCs computed using delta function stimuli resulting in -1 mV and -5 mV perturbations. As the stimulus strength decreases, the directly computed PRCs approach the infinitesimal PRC

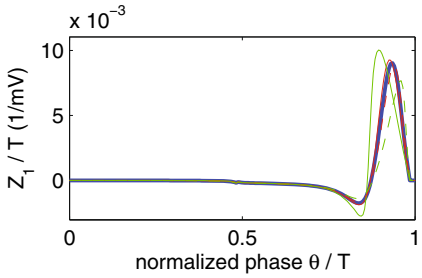

Fig. 14 The effects of perturbation strength on the PRC of a escape-type HCO. The thickest solid line is the infinitesimal PRC as shown in Fig. 2b. The thinner solid lines are the PRCs computed using delta function stimuli resulting in 1 mV and 5 mV perturbations. The thinner dashed lines are the PRCs computed using delta function stimuli resulting in -1 mV and -5 mV perturbations. As the stimulus strength decreases, the directly computed PRCs approach the infinitesimal PRC

Appendix C: PRCs computed using the direct method

In general, the directly measured PRC depends on the strength of the perturbation and its sign (i.e., excitatory vs. inhibitory). However, for sufficiently small perturbations, the PRC would remain unchanged when it is normalized by the amplitude of the perturbation with its sign and would be indistinguishable from the infinitesimal PRC. Figures 13 and 14 compare the PRCs for the release-type HCO and escape-type HCO of the Morris-Lecar-based model for different stimulus strengths. These two figures show that the shape of the infinitesimal PRCs that are directly computed using the adjoint method greatly resemble that of the directly computed PRCs using delta function stimuli that generate up to 5 mV (and possibly beyond) perturbations to the membrane potential.

References

Brown, T.G. (1914). On the nature of the fundamental activity of the nervous centres: together with an analysis of the conditioning of rhythmic avtivity in progression, and a theory of the evolution of function in the nervous system. *Journal of Physiology*, *48*, 18–46.

Brumberg, J.C., & Gutkin, B.S. (2007). Cortical pyramidal cells as non-linear oscillators: experiment and spike-generation theory. *Brain Research*. doi:10.1016/j.brainres.2007.07.028.

Calabrese, R.L. (1995). Half-center oscillators underlying rhythmic movements. In M.A. Arbib (Ed.), *The handbook of brain theory and neural networks* (pp. 444–447). MIT Press.

Clewley, R. (2011). Inferring and quantifying the role of an intrinsic current in a mechanism for a half-center bursting oscillation. *Journal of Biological Physics*. doi:10.1007/s10867-011-9220-1.

Cohen, A.H., Ermentrout, G.B., Kiemel, T., Kopell, N., Sigvardt, K.A., Williams, T.L. (1992). Modelling of intersegmental coordination in the lamprey central pattern generator for locomotion. *Trends in Neuroscience*. doi:10.1016/0166-2236(92)90006-T.

Coombes, S. (2001). Phase locking in networks of synaptically coupled mckean relaxation oscillators. *Physica D: Nonlinear Phenomena*. doi:10.1016/S0167-2789(01)00352-9.

Curtu, R., Shpiro, A., Rubin, N., Rinzel, J. (2008). Mechanisms for frequency control in neuronal competition models. *SIAM Journal on Applied Dynamical Systems*. doi:10.1137/070705842.

Daun, S., Rubin, J.E., Rybak, I.A. (2009). Control of oscillation periods and phase durations in half-center central pattern generators: a comparative mechanistic analysis. *Journal of Computational Neuroscience*. doi:10.1007/s10827-008-0124-4.

Ermentrout, G.B. (1984). Frequency plateaus in a chain of weakly coupled oscillators, i. *SIAM Journal on Mathematical Analysis*, *15*, 215–237.

Gouwens, N.W., Zeberg, H., Tsumoto, K., Tateno, T., Aihara, K., Robinson, H.P.C. (2010). Synchronization of firing in cortical fast-spiking interneurons at gamma frequencies: a phase-resetting analysis. *PLoS Computational Biology*. doi:10.1371/journal.pcbi.1000951.

Grillner, S. (2003). The motor infrastructure: from ion channels to neuronal networks. *Nature Reviews Neuroscience*. doi:10.1038/nrn1137.

Hansel, D., Mato, G., Meunier, C. (1995). Synchronization in excitatory neural networks. *Neural Computation*. doi:10.1162/neco.1995.7.2.307.

Hooper, S.L. (2001). Central pattern generators. *eLS*. doi:10.1038/npg.els.0000032.

Izhikevich, E.M. (2000). Phase equations for relaxation oscillators. *SIAM Journal on Applied Mathematics*. doi:10.1137/S0036139999351001.

Jones, S.R., Mulloney, B., Kaper, T.J., Kopell, N. (2003). Coordination of cellular pattern-generating circuits that control limb movements: the sources of stable differences in intersegmental phase. *Journal of Neuroscience*, *23*, 3457–3468.

Kiehn, O. (2006). Locomotor circuits in the mammalian spinal cord. *Annual Reviews Neuroscience*. doi:10.1146/annurev.neuro.29.051605.112910.

Ko, T.W., & Ermentrout, G.B. (2009). Phase-response curves of coupled oscillators. *Physical Review E*. doi:10.1103/PhysRevE.79.016211.

Kopell, N., & Ermentrout, G.B. (1988). Coupled oscillators and the design of central pattern generators. *Mathematical Biosciences*. doi:10.1016/0025-5564(88)90059-4.

Kristan, W.B., Calabrese, R.L., Friesen, W.O. (2005). Neuronal control of leech behavior. *Progress in Neurobiology*. doi:10.1016/j.pneurobio.2005.09.004.

Kuramoto, Y. (1984). *Chemical oscillations, waves, and turbulence*. Berlin: Springer. doi.wiley.com/10.1002/zamm.19860660706.

LoFaro, T., Kopell, N., Marder, E., Hooper, S.L. (1994). Subharmonic coordination in networks of neurons with slow conductances. *Neural Computation*. doi:10.1162/neco.1994.6.1.69.

Ly, C., & Ermentrout, G.B. (2011). Analytic approximations of statistical quantities and response of noisy oscillators. *Physica D: Nonlinear Phenomena*. doi:10.1016/j.physd.2010.12.004.

Malkin, I.G. (1949). *Methods of Poincare and Liapunov in theory of non-linear oscillations*. Moscow: Gostexizdat.

Mancilla, J.G., Lewis, T.J., Pinto, D.J., Rinzel, J., Connors, B.W. (2007). Synchronization of electrically coupled pairs of inhibitory interneurons in neocortex. *Journal of Neuroscience*. doi:10.1523/JNEUROSCI.2715-06.2007.

Marder, E., & Calabrese, R.L. (1996). Principles of rhythmic motor pattern generation. *Physiological Reviews*, *76*, 687–717.

Morris, C., & Lecar, H. (1981). Voltage oscillations in the barnacle giant muscle fiber. *Biophysical Journal*. doi:10.1016/S0006-3495(81)84782-0.

Mulloney, B., & Hall, W.M. (2007). Local and intersegmental interactions of coordinating neurons and local circuits in the swimmeret system. *Journal of Neurophysiology*. doi:10.1152/jn.00345.2007.

Mulloney, B., & Smarandache, C. (2010). Fifty years of cpgs: two neuroethological papers that shaped the course of neuroscience. *Frontiers in Behavioral Neuroscience*. doi:10.3389/fnbeh.2010.00045.

Mulloney, B., & Smarandache-Wellmann, C. (2012). Neurobiology of the crustacean swimmeret system. *Progress of Neurobiology*. doi:10.1016/j.pneurobio.2012.01.002.

Nadim, F., Zhao, S., Zhou, L., Bose, A. (2011). Inhibitory feedback promotes stability in an oscillatory network. *Journal of Neural Engineering*. doi:10.1088/1741-2560/8/6/065001.

Netoff, T., Schwemmer, M.A., Lewis, T.J. (2012). Experimentally estimating phase response curves of neurons: theoretical and practical issues. In N.W. Schultheiss, A.A. Prinz, R.J. Butera (Eds.), *Phase response curves in neuroscience.* Springer.

Rinzel, J., & Ermentrout, B. (1989). Analysis of neural excitability and oscillations. In C. Koch, & I. Segev (Eds.), *Methods in neuronal modeling: from synapses to networks.* MIT Press.

Rowat, P.F., & Selverston, A.I. (1993). Modeling the gastric mill central pattern generator of the lobster with a relaxation-oscillator network. *Journal of Neurophysiology*, *70*, 1030–1053.

Rowat, P.F., & Selverston, A.I. (1997). Oscillatory mechanisms in pairs of neurons connected with fast inhibitory synapses. *Journal of Computational Neuroscience*. doi:10.1023/A:1008869411135.

Satterlie, R.A. (1985). Reciprocal inhibition and postinhibitory rebound produce reverberation in a locomotor pattern generator. *Science*. doi:10.1126/science.229.4711.402.

Schlichter, T.J. (2011). Modeling the dynamics of central pattern generators and anesthetic action. Ph.D. thesis, University of California, Davis.

Schultheiss, N.W., Prinz, A.A., Butera, R.J. (Eds.) (2012). *Phase response curves in neuroscience.* Springer. doi:10.1007/978-1-4614-0739-3.

Schwemmer, M.A., & Lewis, T.J. (2011). Effects of dendritic load on the firing frequency of oscillating neurons. *Physical Review E*. doi:10.1103/PhysRevE.83.031906.

Schwemmer, M.A., & Lewis, T.J. (2012). The theory of weakly coupled oscillators. In N.W. Schultheiss, A.A. Prinz, R.J. Butera (Eds.), *Phase response curves in neuroscience.* Springer. doi:10.1007/978-1-4614-0739-3_1.

Seely, J., & Chow, C.C. (2011). Role of mutual inhibition in binocular rivalry. *Journal of Neurophysiology*. doi:10.1152/jn.00228.2011.

Sherwood, W.E., & Guckenheimer, J. (2010). Dissecting the phase response of a model bursting neuron. *SIAM Journal on Applied Dynamical Systems*. doi:10.1137/090773519.

Shpiro, A., Curtu, R., Rinzel, J. (2007). Dynamical characteristics common to neuronal competition models. *Journal of Computational Neuroscience*. doi:10.1152/jn.00604.2006.

Skinner, F.K., Kopell, N., Marder, E. (1994). Mechanisms for oscillation and frequency control in reciprocally inhibitory model neural networks. *Journal of Computational Neuroscience*. doi:10.1007/BF00962719.

Smarandache, C., Hall, W.M., Mulloney, B. (2009). Coordination of rhythmic motor activity by gradients of synaptic strength in a neural circuit that couples modular neural oscillators. *Journal of Neuroscience*. doi:10.1523/JNEUROSCI.1744-09.2009.

Smith, J.C., Abdala, A.P.L., Koizumi, H., Rybak, I.A., Paton, J.F.R. (2007). Spatial and functional architecture of the mammalian brain stem respiratory network: a hierarchy of three oscillatory mechanisms. *Journal of Neurophysiology*. doi:10.1152/jn.00985.2007.

Somers, D., & Kopell, N. (1993). Rapid synchronization through fast threshold modulation. *Biological Cybernetics*. doi:10.1007/BF00198772.

Stein, P.S.G. (2007). Motor pattern deletions and modular organization of turtle spinal cord. *Brain Research Reviews*. doi:10.1016/j.brainresrev.2007.07.008.

Taylor, A.L., Cottrell, G.W., Kristan, W.B. (2002). Analysis of oscillations in a reciprocally inhibitory network with synaptic depression. *Neural Computation*. doi:10.1162/089976602317250906.

Varkonyi, P.L., Kiemel, T., Hoffman, K., Cohen, A.H., Holmes, P. (2008). On the derivation and tuning of phase oscillator models for lamprey central pattern generators. *Journal of Computational Neuroscience*. doi:10.1007/s10827-008-0076-8.

Wang, X.J., & Rinzel, J. (1992). Alternating and synchronous rhythms in reciprocally inhibitory model neurons. *Neural Computation*. doi:10.1162/neco.1992.4.1.84.

Williams, T.L., & Bowtell, G. (1997). The calculation of frequency-shift functions for chains of coupled oscillators, with application to a network model of the lamprey locomotor pattern generator. *Journal of Computational Neuroscience*. doi:10.1023/A:1008864410375.

Williams, T.L., Sigvardt, K.A., Kopell, N., Ermentrout, G.B., Remler, M.P. (1990). Forcing of coupled nonlinear oscillators: studies of intersegmental coordination in the lamprey locomotor central pattern generator. *Journal of Neurophysiology*, *64*, 862–871.